Appendix E

SPECIAL CASE STUDY FOR THE ASSESSMENT OF THE CAUSE OF DETERIORATION ON US-23 SOUTH OF FLINT, MICHIGAN

Submitted to the Michigan Department of Transportation

by the Michigan Tech Transportation Institute

Michigan Tech Civil & Environmental Engineering Department

Investigators:

Karl R. Peterson, Research Scientist

Dr. Thomas Van Dam, P.E., Associate Professor

Dr. Lawrence L. Sutter, Assistant Professor

June 30, 2002

Table of Contents

Introduction **3**
Project Description **3**
Experimental Methods **7**
Air-Void System Parameters **7**
Staining for Alkali Silica Reaction **11**
Petrographic Examination **14**
Sodium and Potassium Determination **14**
Sulfate Determination **27**
Discussion **30**
Alkali-Silica Reactivity 31
Dissolution of Calcium Sulfide 32
Other Factors 34
Conclusions **35**

Introduction

Sections of US-23 (referred to in this report as US-23N [CS 25031-30798A]) south of Flint are suffering extensive cracking and joint deterioration in spite of the fact that they were constructed only 10 years ago in 1992. Figures 1 through 4 show typically observed distress manifestations. An adjacent section constructed the following year (referred to as US-23S [CS 25031-31018A]) using comparable design features and materials remains in good condition with little sign of visual distress. In the spring of 2001, the Michigan Department of Transportation (MDOT) sent Michigan Tech a total of 18 cores taken from the pavement for analysis. The cores were representative of four of the mix designs used on US-23N, and two of the mix designs used on US-23S. In order to assess the discrepancy in performance between the US-23N and US-23S sections, a testing regime was developed to investigate several hypotheses that might explain the observed deterioration. Cores from four other pavements with mix designs similar to the pavement south of Flint were also included in this evaluation.

Project Description

The pavement section under study, US-23 south of Flint (CS 25031) is a jointed reinforced concrete pavement (JRCP) with 27 foot transverse joint spacing. The lane widths are 12 foot and are tied to a concrete shoulder. All transverse joints are doweled and longitudinal joints are tied. The slab is 10 inches thick, on a 4-inch thick asphalt treated open graded drainage course (5G crushed concrete) with a 3-inch thick aggregate separator course (22A crushed concrete). The 10-inch thick sand subbase is from the original construction. Underdrains were added in the most recent construction phase.

Table 1 contains information about the locations and conditions of all the pavements sampled. It is noted that cores 19b (CS 50011) and 29a (CS 82291), although from pavements in distressed condition, are older than those from the US-23 (CS 25031) sites. Table 2 contains information about the mix designs from the pavements sampled. Table 3 contains information about the sources of the materials used in the pavements sampled. Appendix A contains specific information regarding the core locations and mix designs for the US-23N and US-23S sections as provided to Michigan Tech by MDOT.

Figure 1. Spall at transverse joint (note paste disintegration).

Figure 2. Cracking running perpendicular to transverse joint.

Figure 3. Complete disintegration of shoulder at transverse joint.

Figure 4. Transverse joint deterioration and map cracking.

Table 1: Location and condition of pavements sampled.

Core ID	Yr. Const.	Route	CS	BMP	EMP	Job #	Direction	Condition
19b	1988/89	M-53	50011	4.8	8.4	25647A	NB	distressed
29a	1976	I-275	82291	2.9	6.0	09902A	NB – exit 11a	distressed
15	1992	US-23	25031	5.9	12.3	30798A	NB	distressed
22	1992	US-23	25031	5.9	12.3	30798A	NB	distressed
32	1992	US-23	25031	5.9	12.3	30798A	NB	distressed
38	1992	US-23	25031	5.9	12.3	30798A	NB	distressed
4a	1992	US-23	25031	5.9	12.3	30798A	SB	distressed
1	1993	US-23	25031	0.0	5.9	31018A	NB	fair
9	1993	US-23	25031	0.0	5.9	31018A	NB	fair
1a	1992	US-23	58034	0.0	6.0	32750A	SB – sec “B”	fair

Table 2: Mix designs from pavements sampled.

Core ID	Cement (kg/m^3)	Water (kg/m^3)	Coarse Agg. (kg/m^3)	Fine Agg. (kg/m^3)	Fly Ash (kg/m^3)	"Sacks Cement"	% Fly Ash
19b	328.0	147.0	1273.5	649.0	0.0	5.9	0
29a	306.0	175.0	846.8	996.2	0.0	5.5	0
15	501.9	166.1	905.9	653.2	0.0	9.0	0
22	284.8	154.3	830.0	920.2	42.7	5.9	13
32	312.1	154.8	830.0	939.8	0.0	5.6	0
38	251.0	120.4	885.8	789.7	83.7	6.0	25
4a	284.8	154.3	859.1	970.6	42.7	5.9	13
1	267.6	169.1	876.3	775.4	67.0	6.0	20
9	390.4	195.8	841.9	755.8	0.0	7.0	0
1a	285.0	162.0	830.0	918.0	43.0	5.9	13

Table 3: Material source information.

Core ID	Cement Source	Fly Ash Source	Coarse Aggregate Type	Inventory Source	Fine Aggregate Type	Inventory Source
19b	no data	no fly ash	slag	no data	natural sand	no data
29a	no data	no fly ash	slag	no data	natural sand	81-57
15	Type I Medusa	no fly ash	slag	82-19	natural sand	63-54
22	Type I Medusa	Detroit Edison Class C	slag	82-19	natural sand	63-54
32	Type I Medusa	no fly ash	slag	82-19	natural sand	63-54
38	Type I Medusa	Detroit Edison Class C	slag	82-19	natural sand	63-54
4a	Type I Medusa	Detroit Edison Class C	slag	82-19	natural sand	63-54
1	Type I St. Mary	US Ash Class F	slag	82-19	natural sand	63-54
9	Type I St. Mary	no fly ash	slag	82-19	natural sand	63-54
1a	Type I/ Medusa	Avon Lake Class F	slag	82-22	natural sand	30-35

In table 1, each pavement was classified as being either in “distressed” condition or “fair” condition. This condition rating is based on observed pavement distress, with distressed sections characterized by spalling, cracking, staining/exudate, or disintegration that is characteristic of MRD. Pavements considered in fair condition have no observed distress consistent with MRD.

Experimental Methods

One core, taken near a transverse pavement joint, was selected from each site. This core was cut in half in a plane parallel to the pavement surface, and the two halves were subsequently cut into slabs in a plane perpendicular to the pavement surface. The following tests were performed on these slabs:

- ASTM C457 Standard Test Method for Microscopical Determination of Parameters of the Air-Void System in Hardened Concrete.
- Chemical staining to detect the presence of secondary sulfate minerals in the entrained air voids.
- Chemical staining to detect alkali-silica reaction (ASR) product.
- Petrographic analysis of thin sections to observe the concrete microstructure.
- Chemical extraction to determine the levels of exchangeable and soluble potassium and sodium.
- Chemical extraction to determine the sulfate levels.

Air-Void System Parameters

One slab from the bottom half of each core was polished and examined under a stereo microscope in accordance with ASTM C457 Procedure B – Modified Point-Count Method. In addition to the standard procedure, the slabs were stained with a solution of potassium permanganate and barium chloride. The chemicals stain sulfate-bearing minerals, such as ettringite, pink. Over time, such minerals commonly occur as secondary growths in the entrained air voids. Often, entrained air voids in deteriorated concrete are completely filled with secondary ettringite. The stain assists in the identification of filled air voids that may otherwise be mistaken for hardened cement paste. In the equations used to determine the air-void system parameters, filled air voids that are identified as paste would be considered to offer no protection to freeze-thaw damage. It is controversial whether filled air voids can protect the paste against freeze-thaw damage, and thus, air-void system parameters are computed for both the concrete in its original state, and the concrete in its existing state.

Tables 4a and 4b summarize the results of the air-void system analysis. Figure 5 shows a chart comparing the spacing factor for the concrete in its original state and the spacing factor in its existing state. A spacing factor in the range of 0.1 to 0.2 mm is considered adequate to provide

freeze-thaw durability. For all cores, the spacing factor increases from the original state to the existing state due to the infilling of many of the air voids by secondary ettringite. Figure 6 consists of a chart comparing the void frequency for the concrete in its original state and in its existing state. For all of the cores, the number of air voids intercepted per unit length of linear traverse decreases from the original state to the existing state. The decrease is due to the complete infilling of many of the air voids by secondary ettringite. Generally, a value of greater than 315 voids intercepted per meter of linear traverse is considered likely to provide good freeze-thaw durability. Figure 7 depicts a typical scene encountered by an operator of an air-void analysis, where many of the smaller air voids are completely filled by ettringite.

Table 4a: Results of ASTM C457 Procedure B – Modified Point-Count Method.

Raw Data	**19b**	**29a**	**4a**	**15**	**22**
area analyzed (cm2)	69.4	100.2	94.9	94.9	69.8
air void stops	133	150	117	117	102
cement paste stops	466	429	294	470	403
coarse aggr. stops	471	449	560	404	474
fine aggr. stops	276	392	361	299	371
ettringite stops	10	5	18	60	15
total stops	1356	1425	1350	1350	1365
traverse length (mm)	3541.9	4363.4	4133.7	4133.7	3565.4
air void intercepts	1066	1878	1318	1751	890
filled air void intercepts	77	404	448	424	465
Results					
vol % coarse aggr.	34.7	31.5	41.5	29.9	34.7
vol % fine aggr.	20.4	27.5	26.7	22.1	27.2
original vol % air voids	10.5	10.9	10.0	13.1	8.6
existing vol % air voids	9.8	10.5	8.7	8.7	7.5
original vol % cement paste	34.4	30.1	21.8	34.8	29.5
existing vol % cement paste	35.1	30.5	23.1	39.3	30.6
original void frequency (voids/m)	323	523	427	526	380
existing void frequency (voids/m)	301	430	319	424	250
original avg. chord length (mm)	0.327	0.208	0.234	0.249	0.226
existing avg. chord length (mm)	0.326	0.245	0.272	0.205	0.299
original air void specific surface (mm^{-1})	12.2	19.2	17.1	16.1	17.7
existing air void specific surface (mm^{-1})	12.3	16.4	14.7	19.6	13.4
original paste/air ratio	3.3	2.8	2.2	2.7	3.4
existing paste/air ratio	3.6	2.9	2.7	4.5	4.1
original spacing factor (mm)	0.266	0.144	0.127	0.165	0.194
existing spacing factor (mm)	0.292	0.177	0.181	0.226	0.307

Table 4b: Results of ASTM C457 Procedure B – Modified Point-Count Method.

Raw Data	**32**	**38**	**1**	**9**	**1A**
area analyzed (cm2)	94.9	94.9	70.0	72.9	94.9
air void stops	120	126	100	150	116
cement paste stops	365	358	300	429	304
coarse aggr. stops	485	437	571	449	534
fine aggr. stops	380	415	396	392	387
ettringite stops	0	14	1	5	9
total stops	1350	1350	1368	1425	1350
traverse length (mm)	4133.7	4133.7	3573.2	3722.1	4133.7
air void intercepts	1466	1765	824	1878	1275
filled air void intercepts	290	331	137	404	170
Results					
vol % coarse aggr.	35.9	32.4	41.7	31.5	39.6
vol % fine aggr.	28.1	30.7	28.9	27.5	28.7
original vol % air voids	8.9	10.4	7.4	10.9	9.3
existing vol % air voids	8.9	9.3	7.3	10.5	8.6
original vol % cement paste	27.0	26.5	21.9	30.1	22.5
existing vol % cement paste	27.0	27.6	22.0	30.5	23.2
original void frequency (voids/m)	425	507	269	613	350
existing void frequency (voids/m)	355	427	231	505	308
original avg. chord length (mm)	0.209	0.205	0.275	0.177	0.265
existing avg. chord length (mm)	0.251	0.219	0.317	0.209	0.279
original air void specific surface (mm^{-1})	19.1	19.6	14.6	22.5	15.1
existing air void specific surface (mm^{-1})	16.0	18.3	12.6	19.2	14.4
original paste/air ratio	3.0	2.6	3.0	2.8	2.4
existing paste/air ratio	3.0	3.0	3.0	2.9	2.7
original spacing factor (mm)	0.159	0.131	0.204	0.123	0.161
existing spacing factor (mm)	0.191	0.161	0.239	0.151	0.188

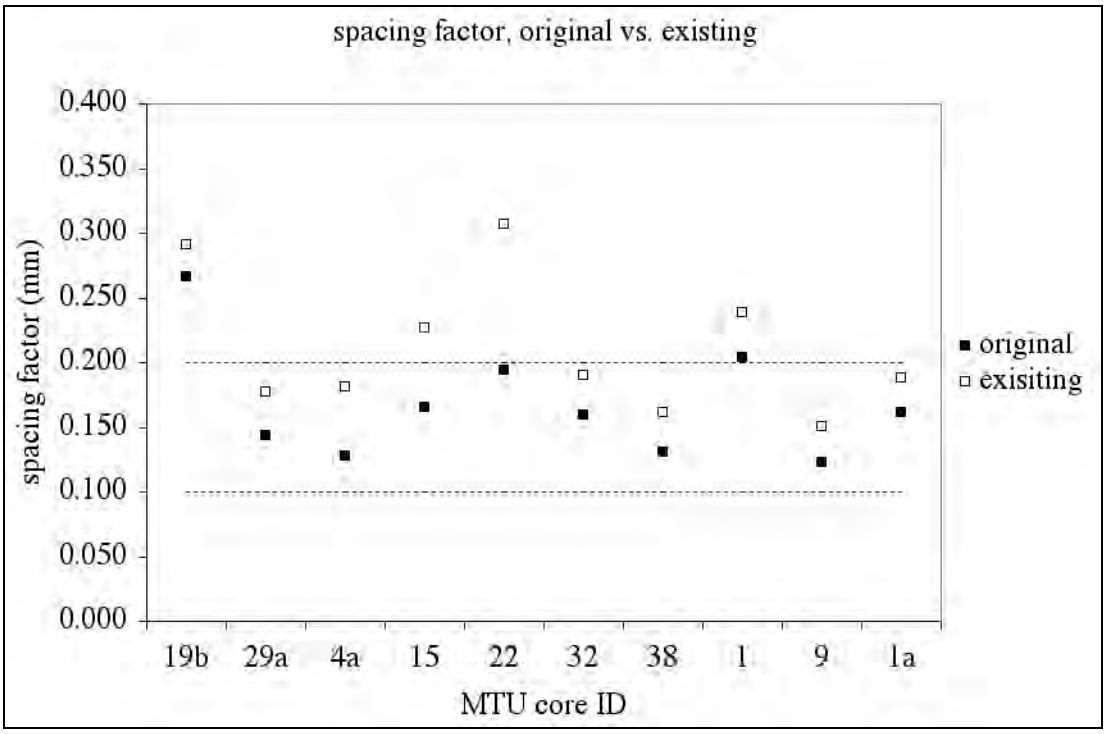

Figure 5: Chart depicting increase in spacing factor due to infilling of air voids by secondary ettringite. Dashed lines represent accepted range for freeze-thaw durability.

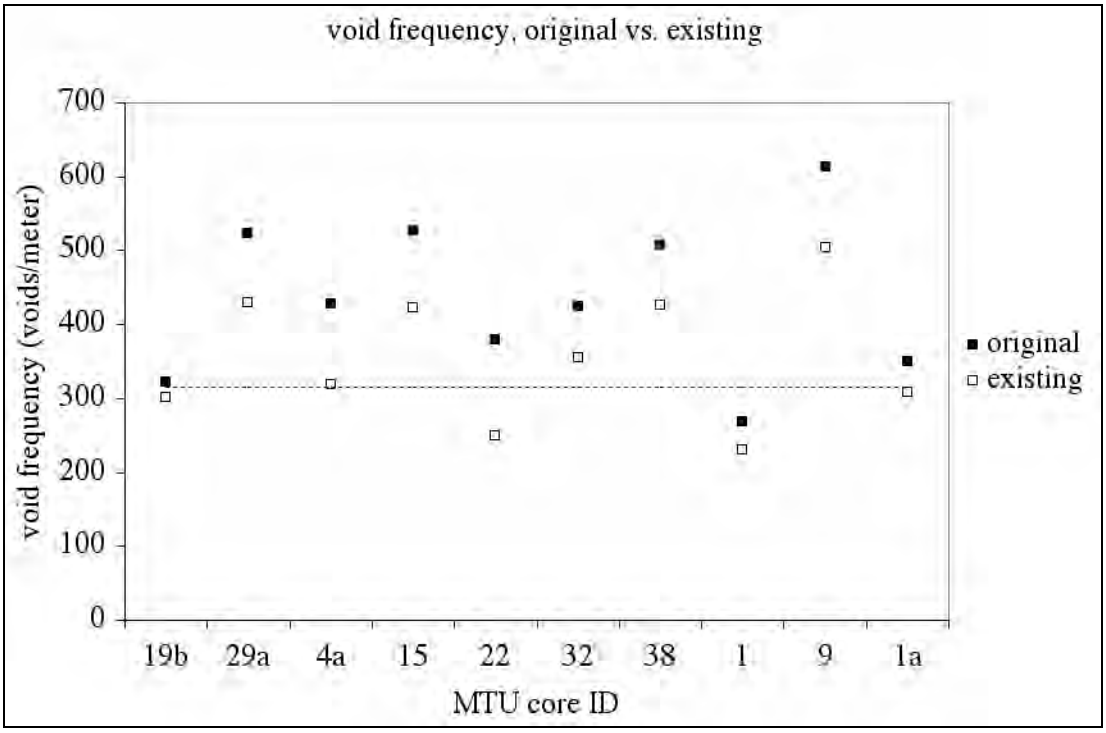

Figure 6: Chart depicting decrease in the number air voids intercepted per meter of linear traverse due to infilling of air voids by secondary ettringite. Values above dashed line are considered likely to ensure good freeze-thaw durability.

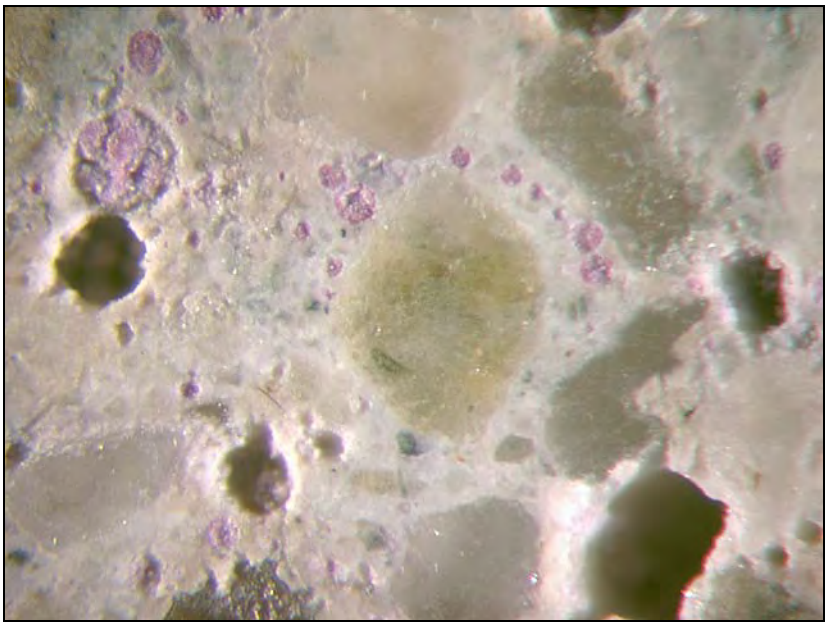

Figure 7: Microscope image of polished slab surface from core 29a (CS 82291) stained for sulfate minerals. Ettringite filled air voids are stained pink, magnified 83x.

Staining for Alkali Silica Reaction

One slab representing the top half of each core was polished and stained with a solution of sodium cobaltinitrite. The stain turns potassium bearing alkali silica gel yellow. In all the samples evaluated, some chert particles in the fine aggregate were stained yellow. Uniquely, in the pavements classified to be in distressed condition, the stained chert particles were also consistently cracked, often with cracks extending into the cement paste and interconnecting with other cracked chert particles. This was in contrast to the pavements classified to be in good condition, where the chert particles were stained yellow, but rarely exhibited any cracking. Figures 8a and 8b show a cracked chert particle typical of the pavements in distressed condition. Figures 9a and 9b show a chert particle that has picked up the yellow stain, but does not show cracking, typical of the pavements in good condition. It is extremely rare to find chert particles showing cracking in the fair sections versus almost universal cracking, with associated copious quantities of ASR reaction product, observed in the chert particles from cores obtained from the distressed sections. Although the difference between the distressed and fair sections is striking, it is noted that the “fair” sections are relatively young in age being constructed in 1993 and it is possible that deterioration may occur as they age.

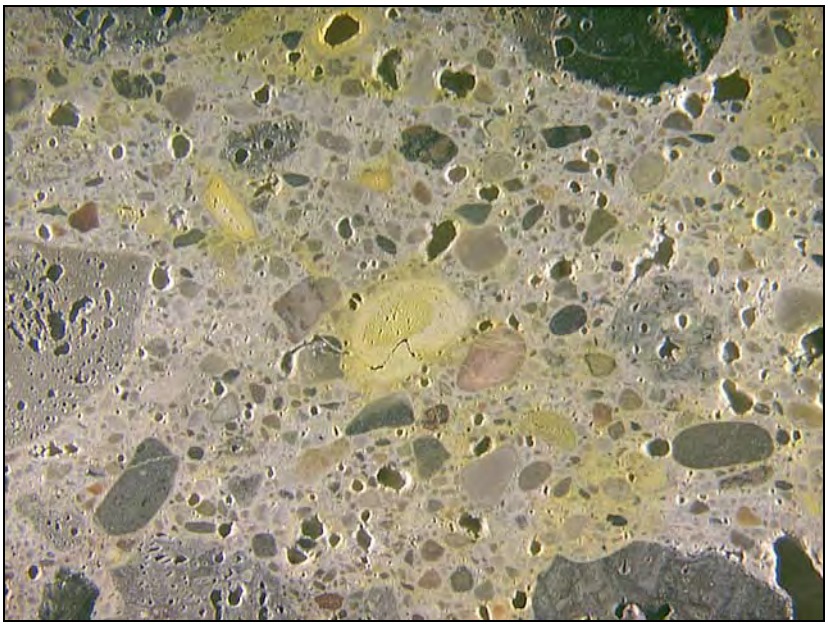

Figure 8a: Close-up of a polished and stained surface from core 22 (CS 25031-30798A). Alkali-silica reactive stained particles appear yellow and exhibit cracking, magnified 6x.

Figure 8b: A close-up of Figure 8a, showing cracked reactive chert particle, with cracks propagating through neighboring non-chert sand particles, magnified 15x.

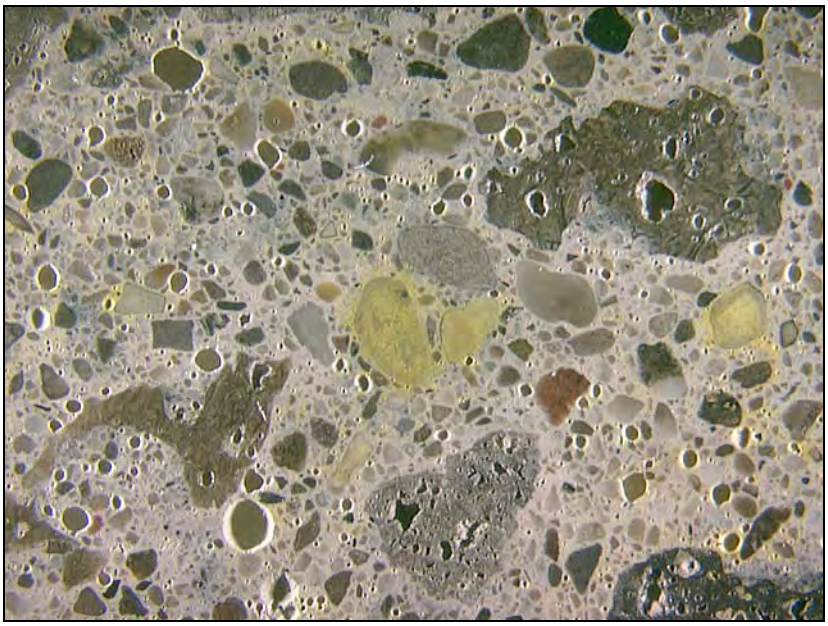

Figure 9a: Close-up of a polished and stained surface from core 9 (CS 25031-31018A). Alkali-silica reactive stained particles appear yellow but do not exhibit cracking, magnified 6x.

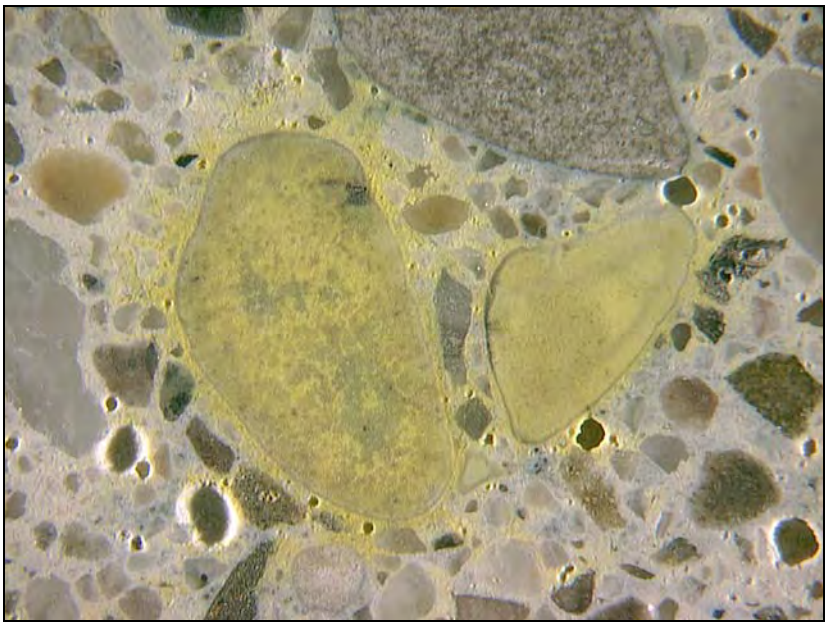

Figure 9b: A close-up of Figure 9a, showing yellow stained reactive chert particle, and the absence of any related cracking, magnified 15x.

Petrographic Examination

Fluorescent epoxy impregnated thin sections were made using slabs from each of the cores. At least four thin sections were made to represent each core, one directly at the pavement surface, one at the contact with the sub-base, and two or more at intermediate depths. Figures 10 through 16 show examples of the cracked reactive chert particles that are abundant in the cores from poorly performing sections. Cracks and air voids filled with alkali silica gel are often associated with these cracked chert particles. Figures 17 through 19 show examples of the reactive chert, but without the accompanying cracks and gel deposits, as is typical for the cores obtained from pavements in fair condition.

Sodium and Potassium Determination

Given the prevalence of alkali silica reactive chert, an effort was made to determine the alkali content of the concrete in the various pavements. Since there were no records available for alkali content in the fly ash and cement, and no standard method available for determining available alkalis in hardened concrete, an extraction technique developed for the determination of exchangeable and soluble sodium and potassium in soils was adopted. The slabs from each core were crushed to a fine powder, and the alkalis were extracted with an ammonium acetate solution. The concentrations of potassium and sodium were determined by an inductively coupled plasma emission spectrophotometer. The results from the test are expressed in weight percent elemental sodium and weight percent elemental potassium. In Table 6, the results were converted to the industry convention of kilograms of "Na_2O equivalent" per cubic meter of concrete, based on the total mass from the mix designs, with the exception of core 4a (CS 25031-30798A), which had no mix design information available. In this case, an approximation was used based on the mix design from core 22 (CS 25031-30798A).

The recalculation to kilograms of "Na_2O equivalent" per cubic meter of concrete allows comparisons to be made with industry standards for limiting total alkalis in the mixture. The Canadian standards specifying a maximum of 3.0 kg/m^3 Na_2O equivalent for mild protection, 2.2 kg/m^3 Na_2O equivalent for moderate protection, and 1.7 kg/m^3 Na_2O equivalent for strong protection. As can be seen in Table 6, two of the distressed sections are above the recommended limits for "mild" protection whereas all three "fair" performing pavements are below the limit for "strong" protection.

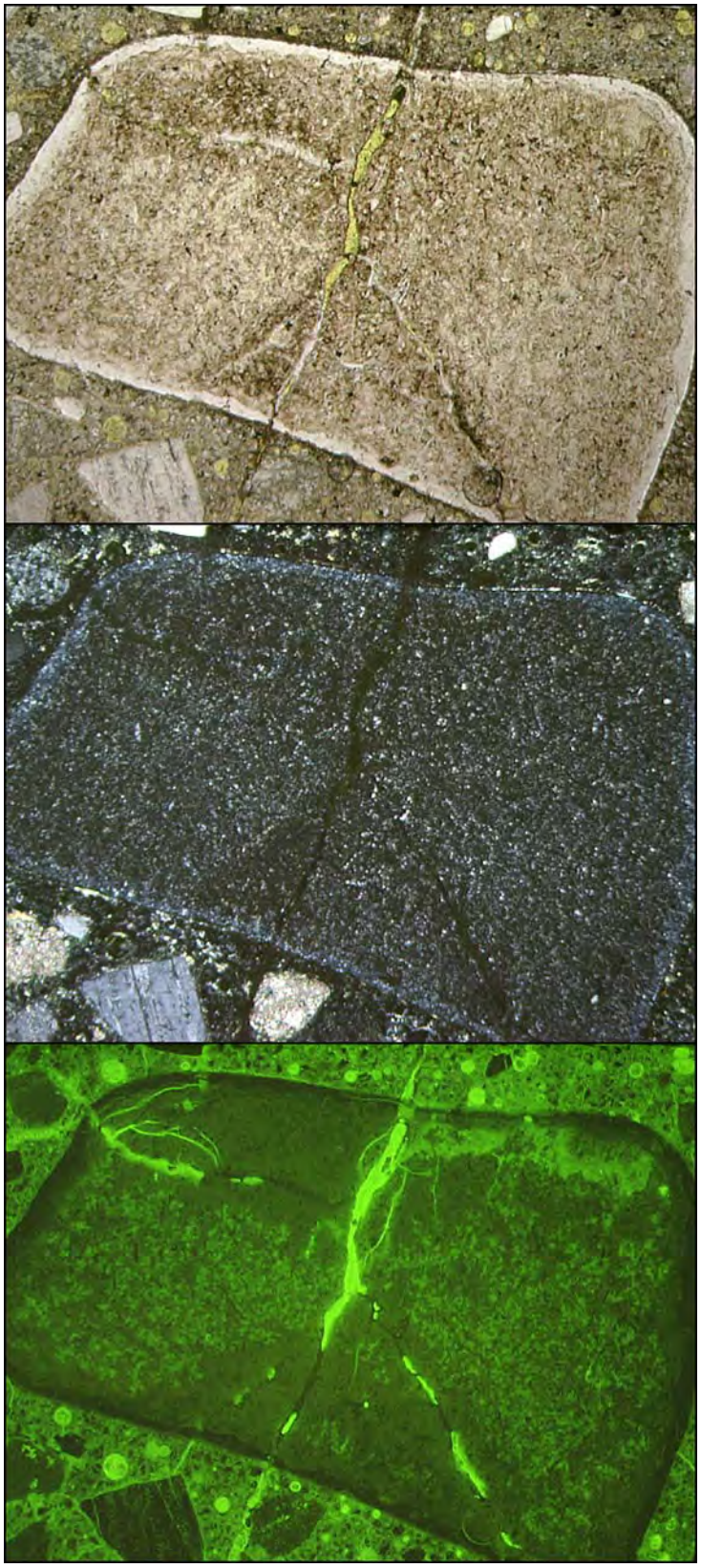

Figure 10: Example of cracked reactive chert from core 19b (CS 50011), magnified 40x. From top to bottom, plane polarized light, cross polarized light, and epifluorescent illumination.

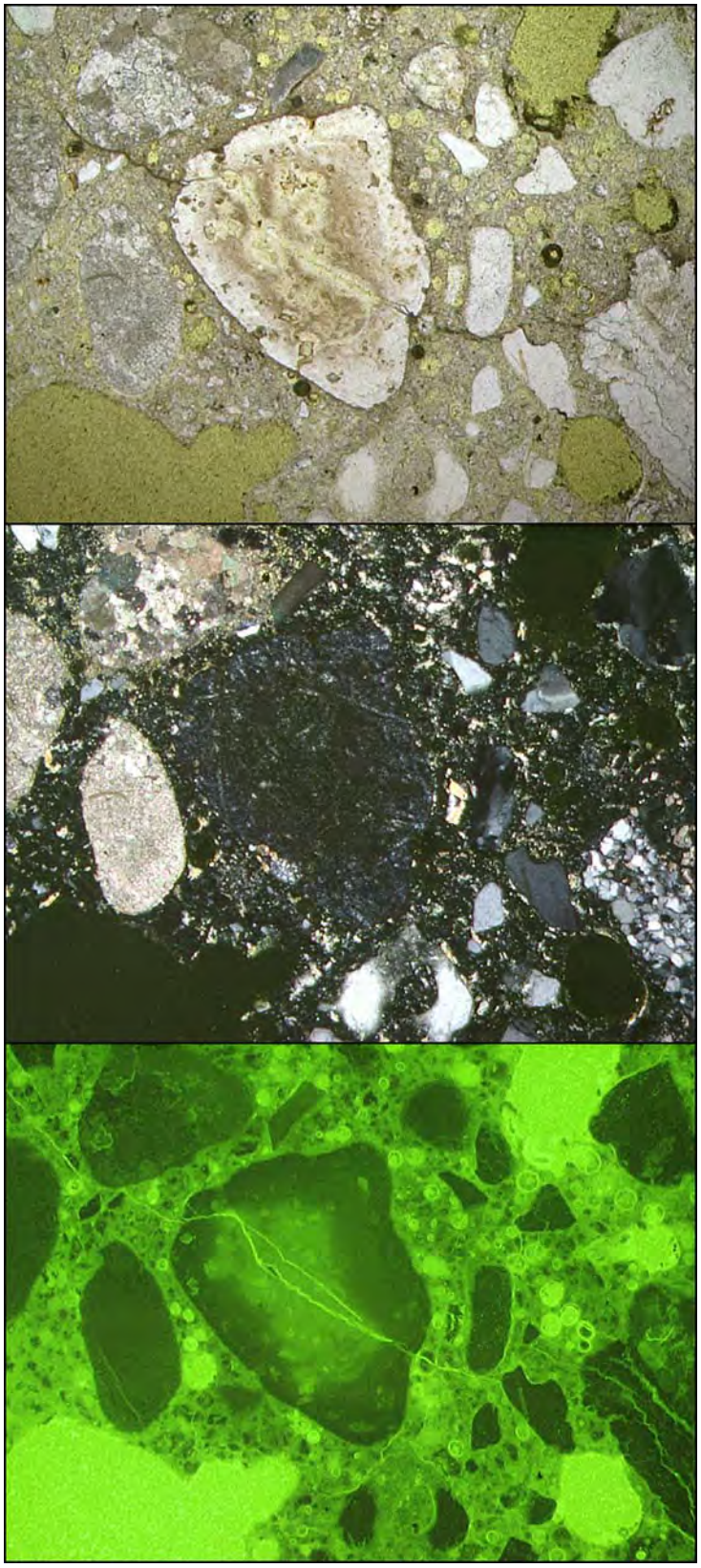

Figure 11: Example of cracked reactive chert from core 29a (CS 82291), magnified 40x. From top to bottom, plane polarized light, cross polarized light, and epifluorescent illumination.

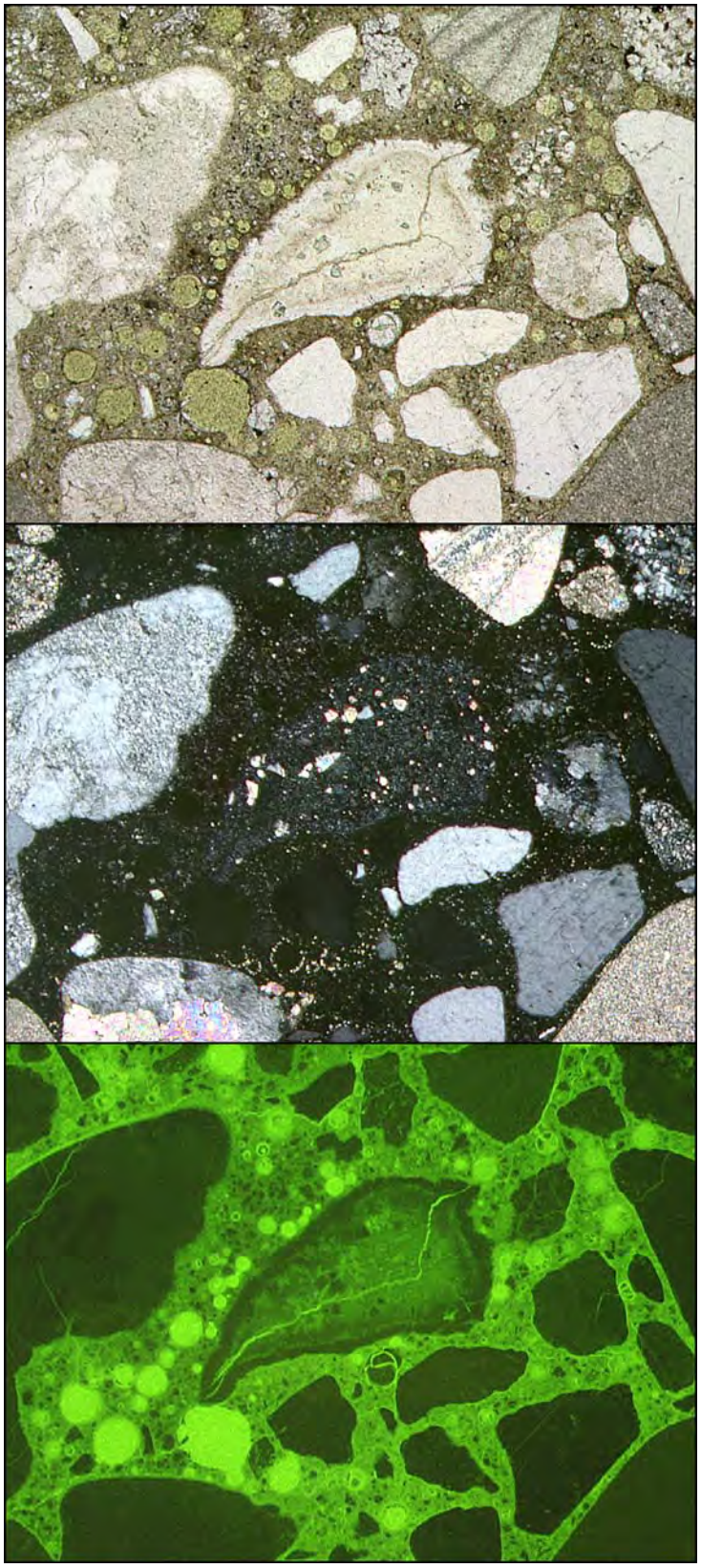

Figure 12: Example of cracked reactive chert from core 4a (CS 25031-30798A), magnified 40x. From top to bottom, plane polarized light, cross polarized light, and epifluorescent illumination.

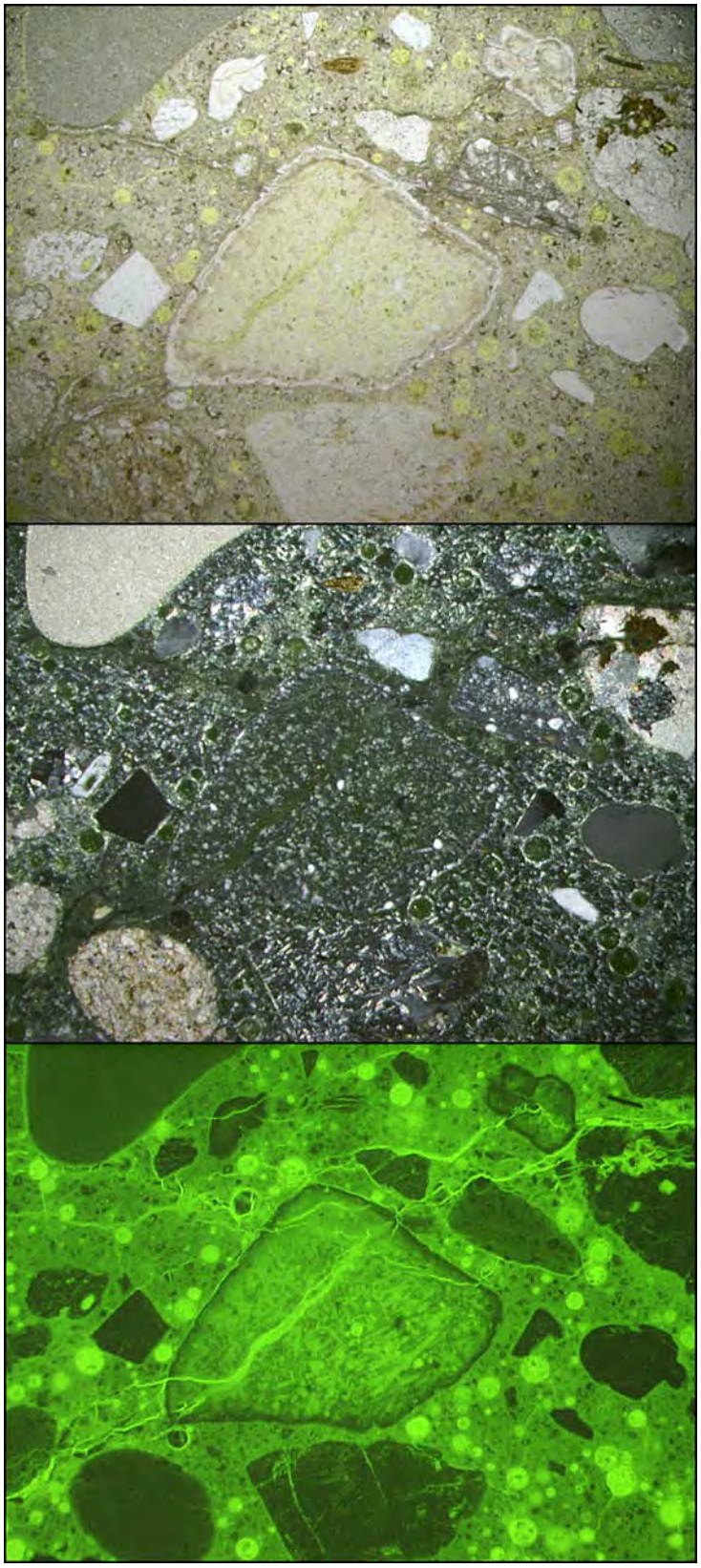

Figure 13: Example of cracked reactive chert from core 15 (CS 25031-30798A), magnified 40x. From top to bottom, plane polarized light, cross polarized light, and epifluorescent illumination.

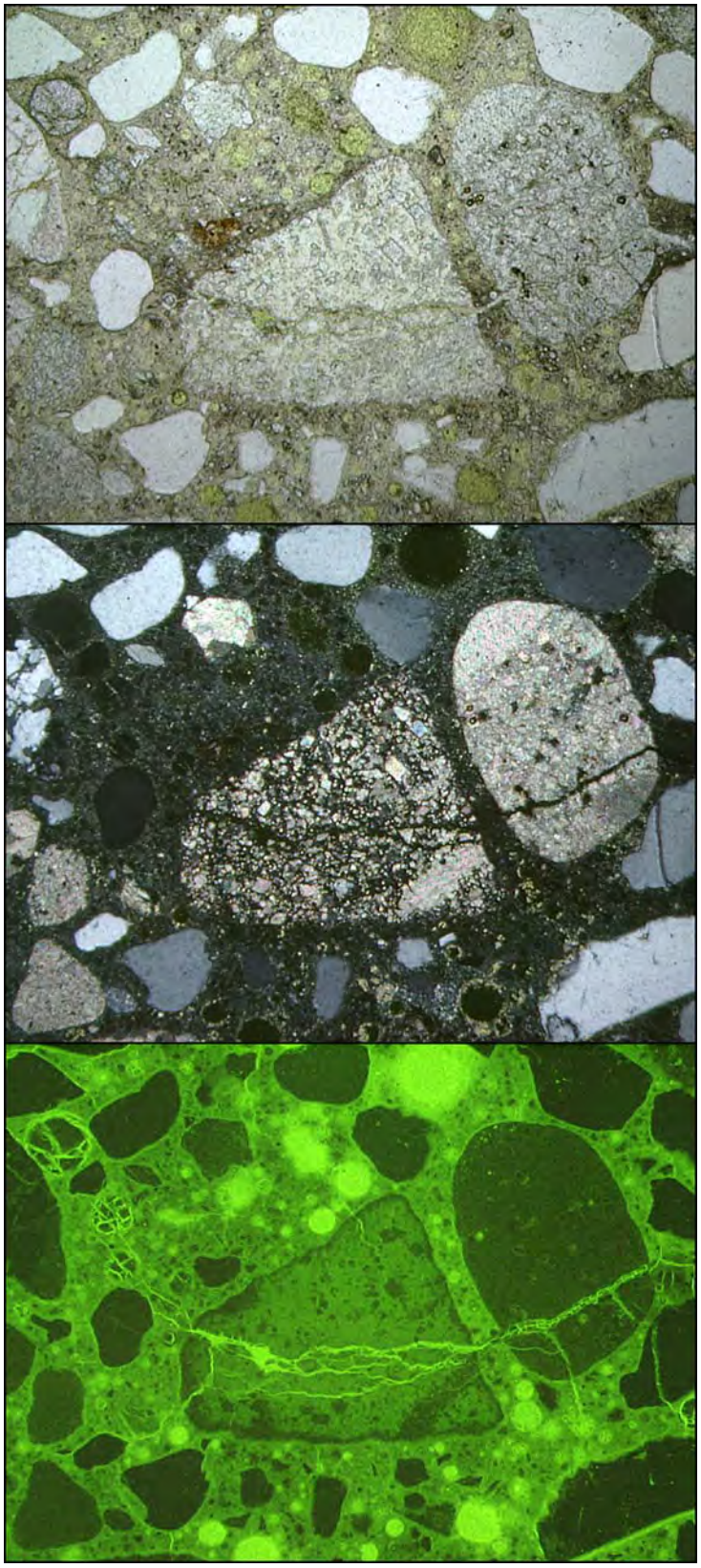

Figure 14: Example of cracked reactive chert from core 22 (CS 25031-30798A), magnified 40x. From top to bottom, plane polarized light, cross polarized light, and epifluorescent illumination.

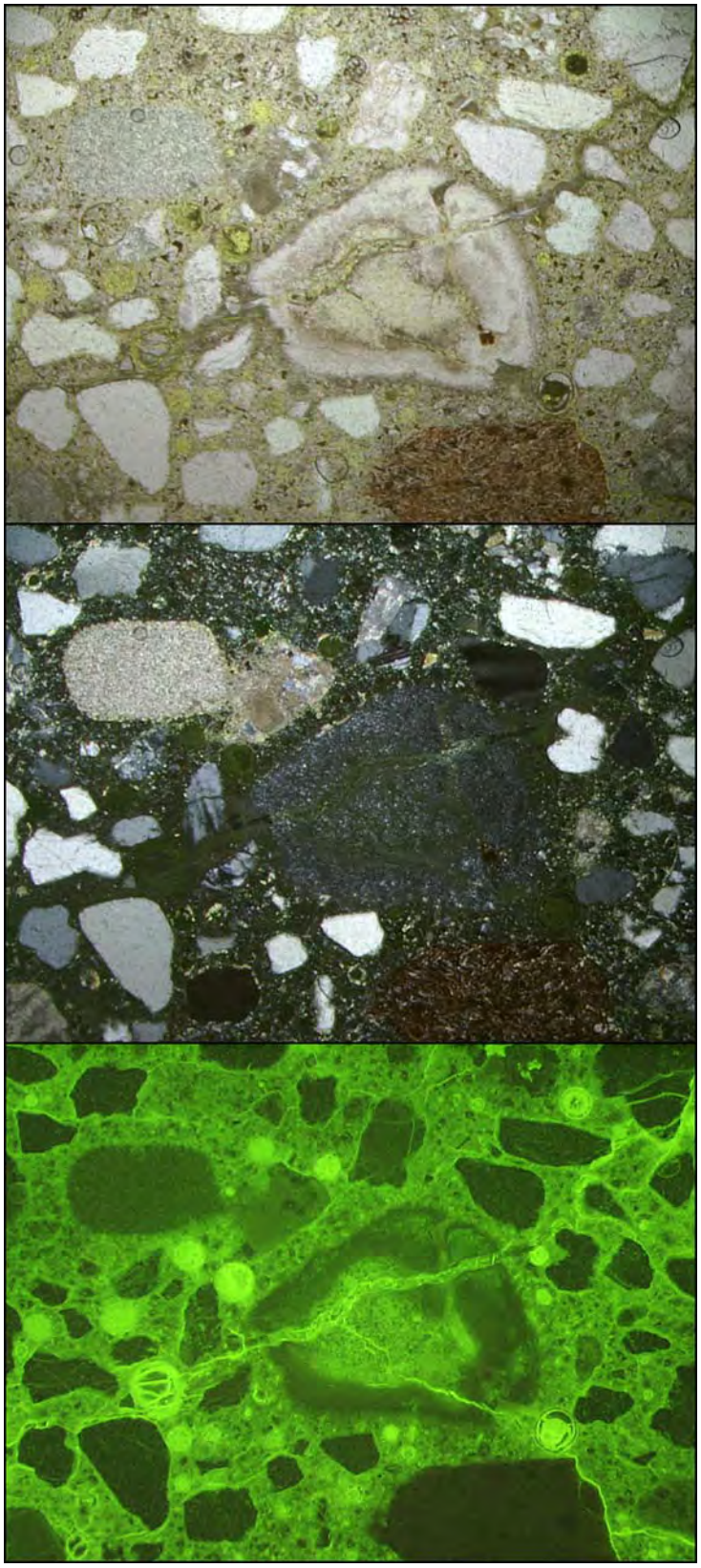

Figure 15: Example of cracked reactive chert from core 32 (CS 25031-30798A), magnified 40x. From top to bottom, plane polarized light, cross polarized light, and epifluorescent illumination.

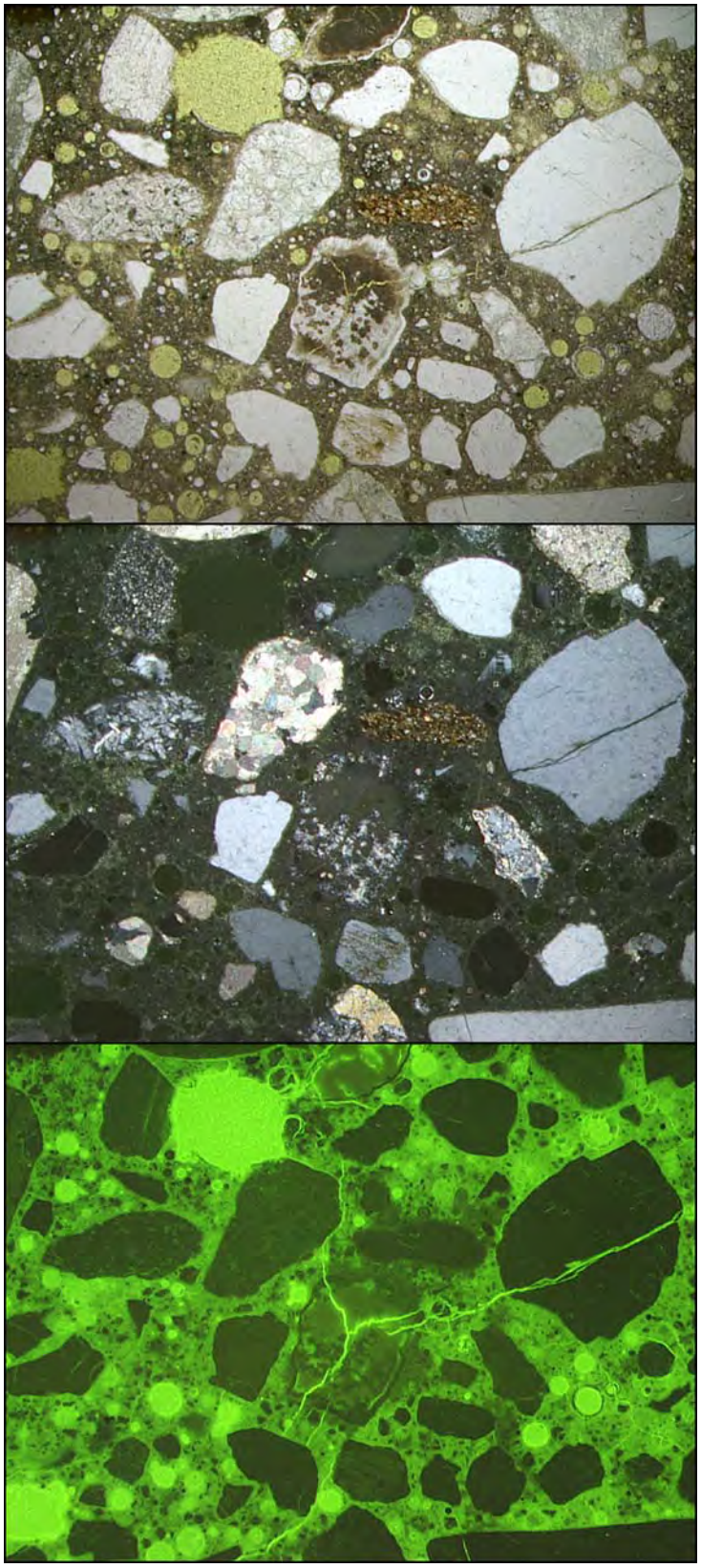

Figure 16: Example of cracked reactive chert from core 38 (CS 25031-30798A), magnified 40x. From top to bottom, plane polarized light, cross polarized light, and epifluorescent illumination.

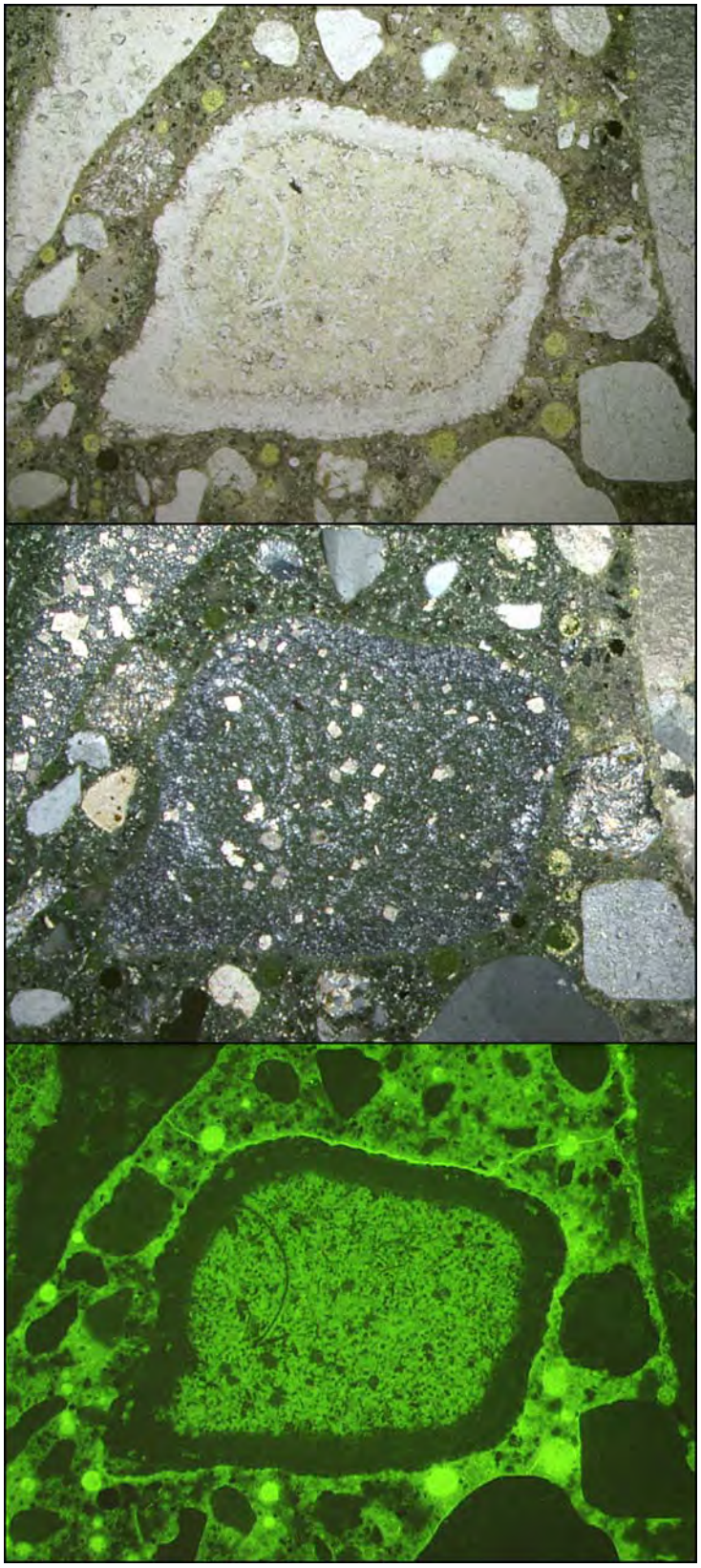

Figure 17: Example of reactive chert from core 1 (CS 25031-31018A), magnified 40x. From top to bottom, plane polarized light, cross polarized light, and epifluorescent illumination.

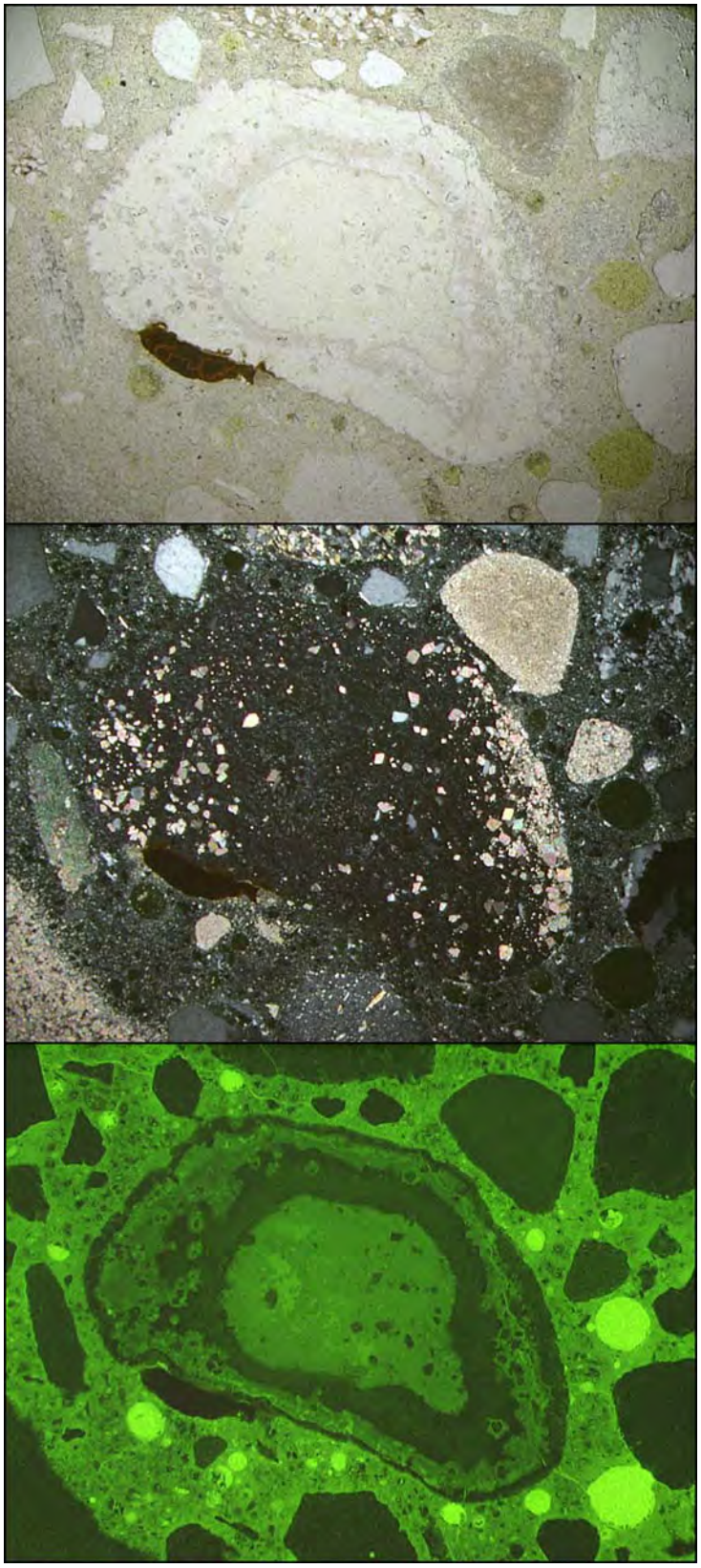

Figure 18: Example of reactive chert from core 9 (CS 25031-31018A), magnified 40x. From top to bottom, plane polarized light, cross polarized light, and epifluorescent illumination.

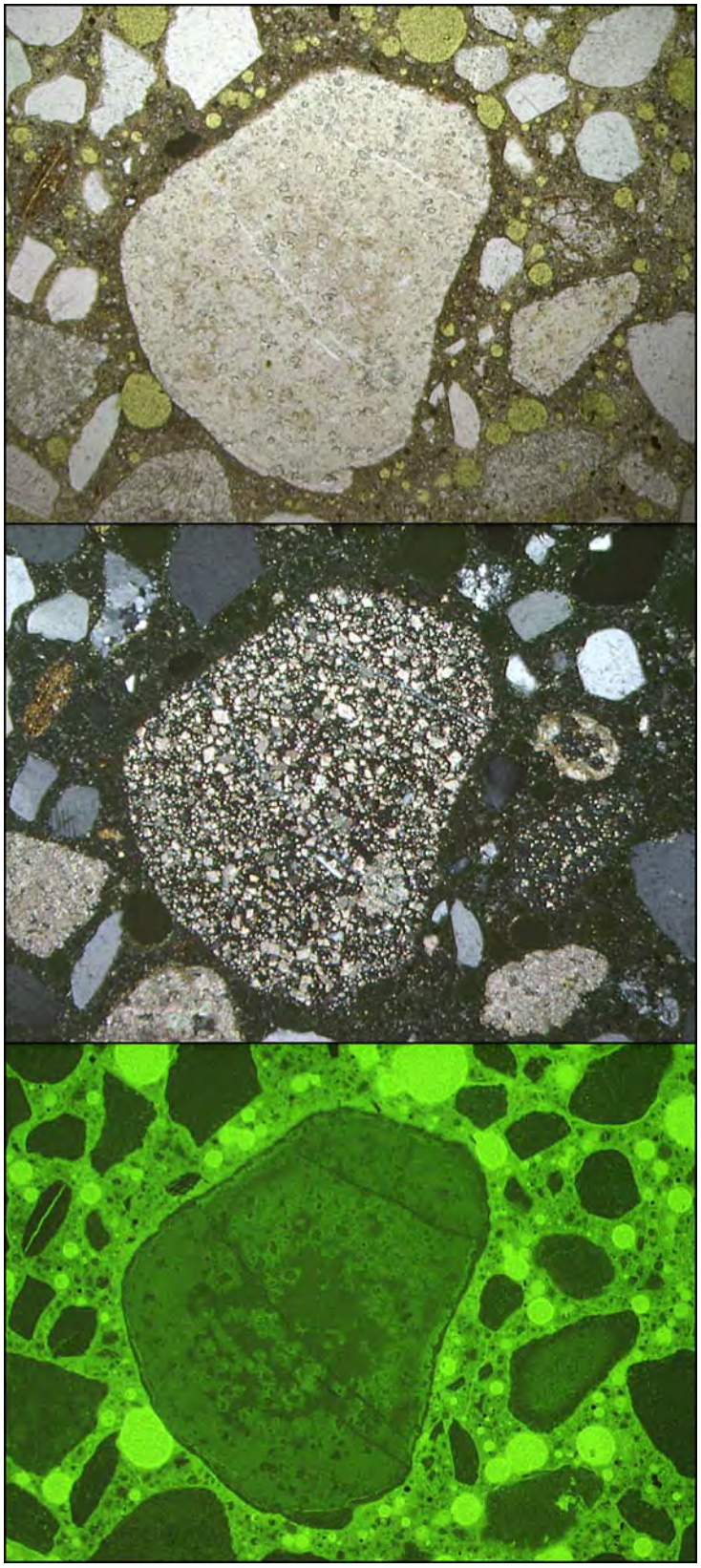

Figure 19: Example of reactive chert from core 1a (CS 58034), magnified 40x. From top to bottom, plane polarized light, cross polarized light, and epifluorescent illumination.

Table 6: Results of alkali extraction, combined with basic mix design information.

Core ID	Sacks of Cement	Percent Fly Ash	kg/m^3 $Na_2$0 Equivalent	Condition	Canadian Alkali Limit
19b	5.9	0	1.9	distressed	“moderate” protection
29a	5.5	0	1.6	distressed	“strong” protection
15	9.0	0	2.1	distressed	“moderate” protection
22	5.9	13	3.1	distressed	above “mild” protection
32	5.6	0	1.7	distressed	“moderate” protection
38	6.0	25	4.3	distressed	above “mild” protection
4a	5.9	13	2.0	distressed	“moderate” protection
1	6.0	20	1.3	fair	“strong” protection
9	7.0	0	1.1	fair	“strong” protection
1a	5.9	13	1.5	fair	“strong” protection

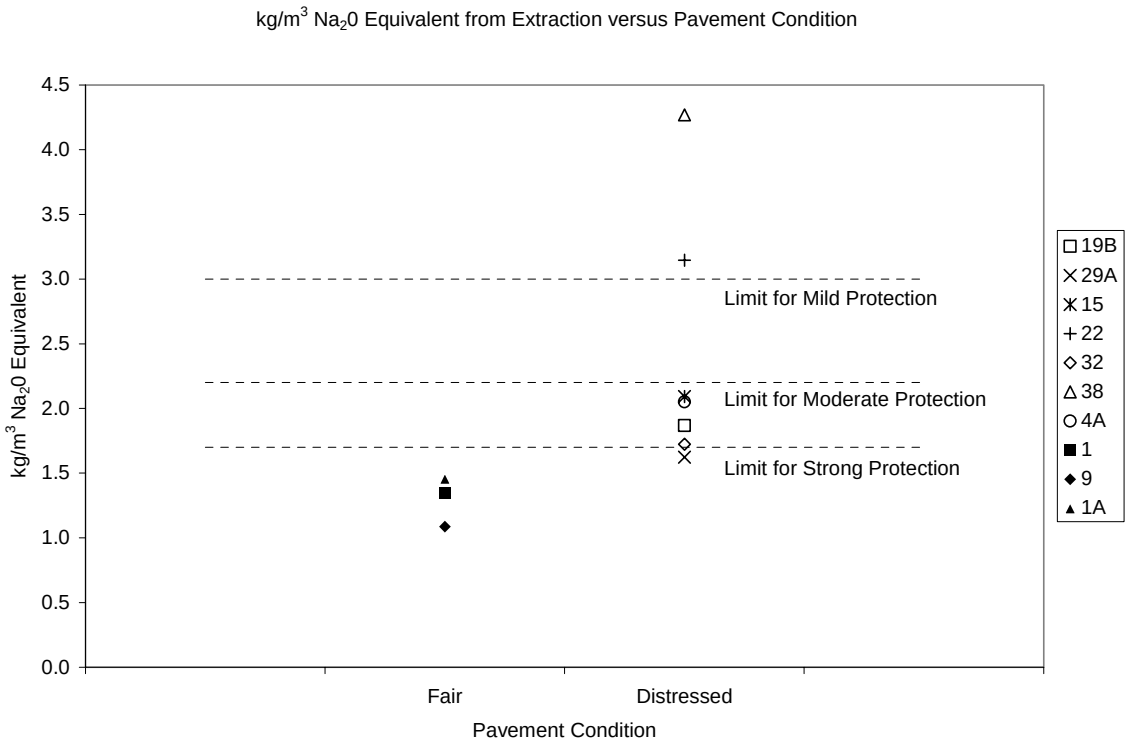

Figure 20: Available alkalis plotted against pavement condition.

Figure 20 depicts the results presented in Table 6 in terms of pavements in fair or distressed condition. Note that all the cores from pavements in fair condition had alkali levels below the limit for strong protection whereas all but one pavement in distressed condition exceeded this limit. Interestingly, the two cores with the highest alkali levels (38 and 22 [both CS 25031-30798A]) both contained a Detroit Edison Class C fly ash and the Medusa Type I cement. Although alkali test data on the fly ash is not available, it is common for Class C fly ashes to have fairly high alkali contents. Tied for the third highest measured total alkali content was core 4a (CS 25031-30798A), which is also suspected of containing the Detroit Edison Class C fly ash, although the specific mix design information is unknown. Core 4a was obtained from a distressed performing section on US-23N. Cores containing Class F fly ash (core 1 [CS 25031-31018A and core 1a [CS 58034]) were both from fair performing pavement sections and had low alkali levels.

This analysis suggests that the type and amount of fly ash may be contributing to the total amount of alkalis measured in the concrete, and to some degree, the amount of deterioration observed. It appears that concrete mixtures containing Class C fly ash have higher total alkalis than similar mixtures made with cement alone. It is also observed that mixtures made with the Class F fly ash have low alkali levels and little evidence of deleterious ASR as indicated by observed fracturing of chert particles or the presence of alkali-silica reaction product. But neither the total alkali content nor the presence of Class C fly ash can be primarily responsible for the observed deterioration. One section that contains no fly ash is suffering the most severe deterioration from the US-23N project (i.e. the section from which core 15 [CS 25031-30798A] was obtained) while the section with the highest total alkali content (from which core 38 [CS 25031-30798A] was obtained) has the least visible distress of the US-23N project. It is noted though that all of the cores obtained from the US-23N project have significant amounts of microcracking emanating from reacting chert particles, and it is likely only a matter of time before all sections progress towards serious distress.

Sulfate Determination

Secondary ettringite deposits in air voids are a common feature for all the cores evaluated in this study. Previous research conducted at Michigan Tech has indicated that calcium sulfide present in blast furnace slag aggregate may dissolve and oxidize to become a source of sulfate and calcium in the concrete, perhaps encouraging the formation of ettringite in the entrained air voids. A gravimetric procedure of sulfate determination was used according to British Standard 1881:Part 124. Methods for Analysis of Hardened Concrete: 1988. The weight percent SO_3 computed from the mix design assumes 3.5% by weight SO_3 for the cement and 4.5% by weight of the fly ash. The results of the sulfate determinations, expressed in terms of SO_3, are presented in Table 7. Graphical representations of the results are presented in Figures 21 and 22.

Table 7: Results of sulfate analysis.

Core ID	Wt% SO_3 computed from mix design	Wt% SO_3 from extraction	Difference	Percent Excess SO_3 Above Computed	Condition
19b	0.48	0.68	0.20	41.1	distressed
29a	0.46	0.57	0.11	24.5	distressed
15	0.79	1.02	0.23	29.3	distressed
22	0.53	0.65	0.11	21.2	distressed
32	0.49	0.66	0.17	34.5	distressed
38	0.59	0.75	0.16	27.4	distressed
4a	0.53	0.67	0.14	25.6	distressed
1	0.57	0.65	0.07	12.9	fair
9	0.63	0.74	0.11	18.3	fair
1a	0.53	0.61	0.08	14.3	fair

It is noted that in all cases, the extraction of sulfate from field specimens exceeded the calculated sulfate levels. This is not unexpected since the calculated sulfate levels were based solely on the assumed sulfate in the cement and fly ash, and did not consider possible additional sulfates from aggregate and other sources. Table 7 presents the difference between the extracted weight percent SO_3 and the computed value and the percent difference that the extracted amount is above the computed. Figure 23 is a plot relating the percent excess SO_3 above the computed value to the pavement condition. Statistical analysis using a t-test finds that a significant difference exists between the excess SO_3 for pavements in fair and distressed conditions.

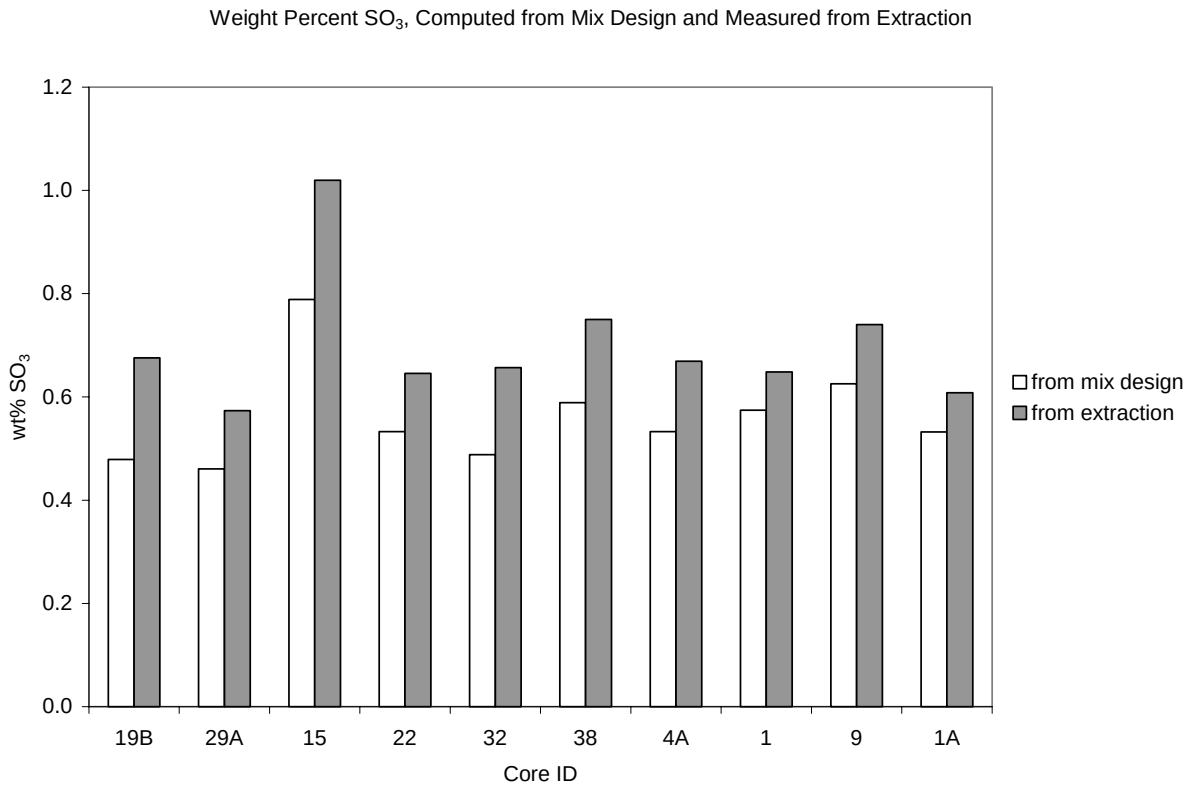

Figure 21. Results of sulfate analysis.

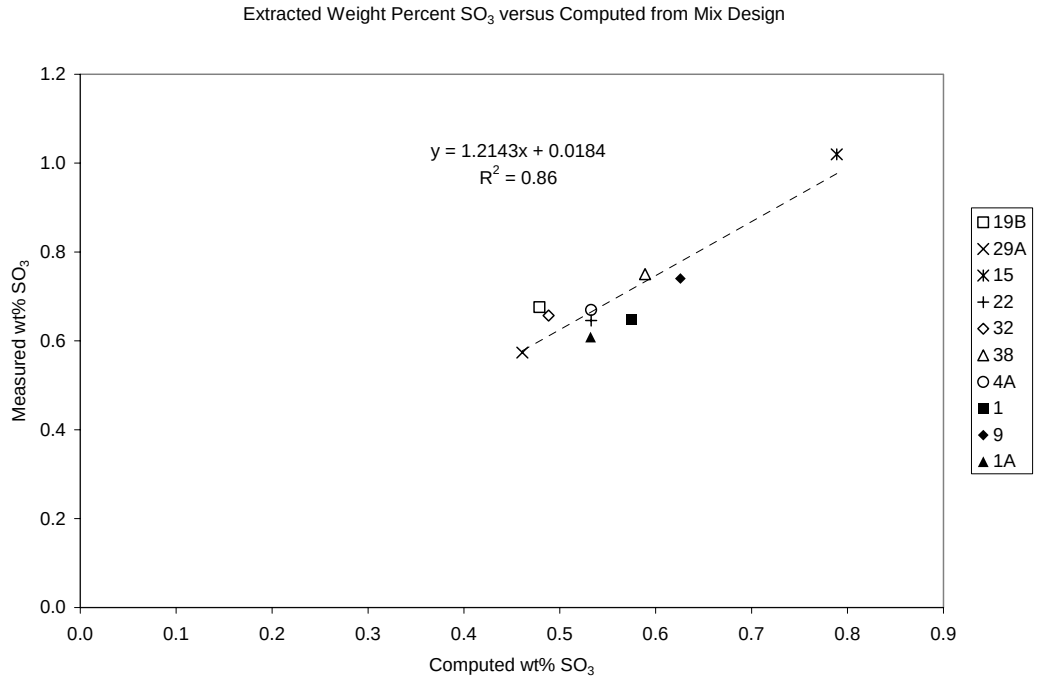

Figure 22. Relationship between measured and computed weight percent SO_3.

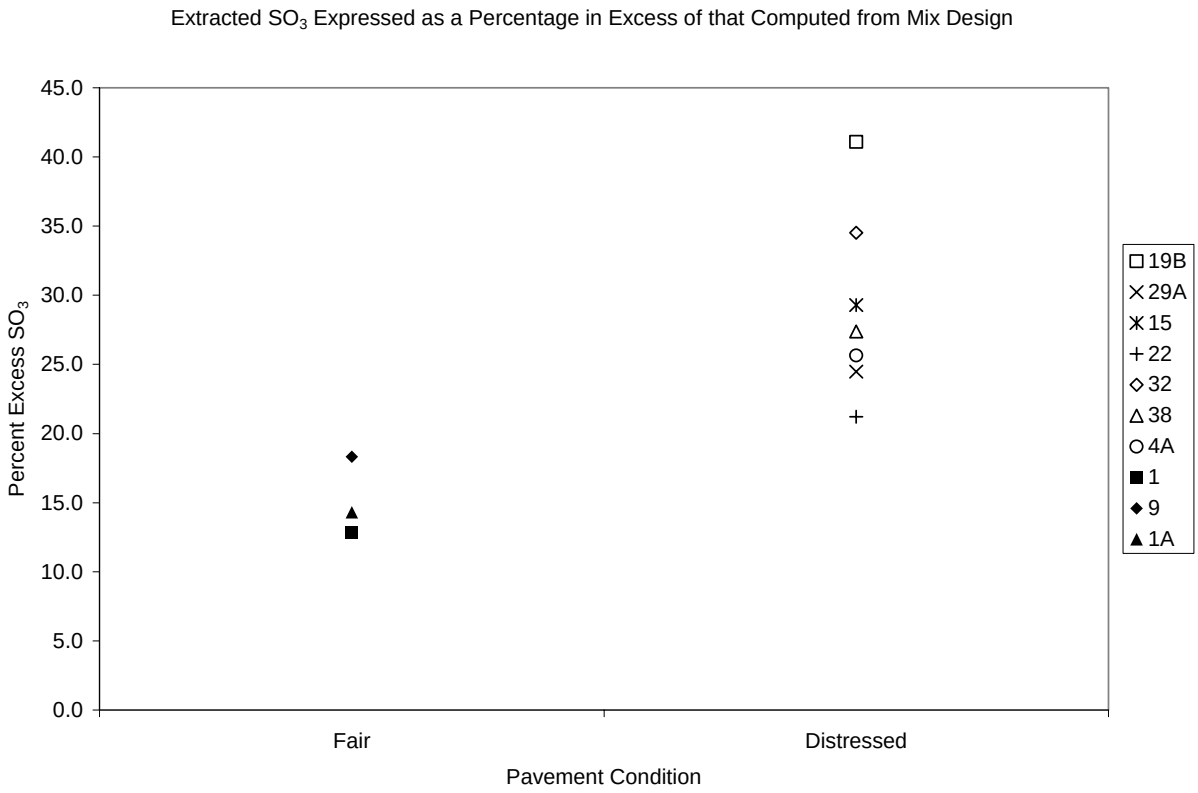

Figure 23. Percent excess SO_3 versus pavement condition.

The sulfate analysis indicates that the concentration of SO_3 in all of the pavements sampled is in excess of that computed. Potential sources of the "excess" sulfate include the likelihood of some error in the assumptions regarding the sulfate levels in the cement and fly ash, although the values selected were selected at the high end of the common range. It is also possible that sulfates in the mix water also added to the total, but it is not likely that this was a significant factor. It is also possible that sulfates may have migrated into the concrete after placement, either through contaminated ground water (very unlikely in these locations) or through deicing salts contaminated with sulfates such as gypsum. Another potential source of excess internal sulfates is the aggregate, slag being the most likely potential contributor. The "excess" sulfates might also be an artifact of the test procedure itself. For these reasons, the data presented focuses more on the percent SO_3 in excess of the predicted amount instead of the absolute values measured.

The effect of the excess sulfates on concrete durability cannot be easily predicted. In the worst case, excess sulfates will react with the hydrated cement paste resulting in sulfate attack. But it is almost impossible to assess the potential for this occurrence for these mixtures because other factors including cement chemistry, the water-to-cement ratio, and concrete permeability will impact the sulfate resistance of the concrete. Further, the presence of admixtures/additives also complicates the situation, particularly the use of the Class C fly ash, which is known to have quite variable effects on the sulfate resistance of concrete[1], at times improving it but on other occasions having a negative impact. Due to all these uncertainties, it is impossible to say at what concentration the excess sulfates might result in sulfate attack.

But it is telling that a statistically significant relationship exists between the excess sulfates and the condition of the pavements. Pavements classified as being distressed have higher percent excess sulfates than those classified as being in fair condition. This is an indication that the excess sulfates may be related to the observed distress.

Discussion

The answer to the question of why US-23N (CS 25031-30798A) is deteriorating prematurely is unclear. It is known that distress was observed on these sections, particularly the cross-over lanes constructed with a high cement content concrete (9 sack mixtures), at a very early age, initially indicating that plastic shrinkage or drying shrinkage cracking might be to blame. There is also evidence, based on discussions with MDOT engineers, that the slag coarse aggregate stockpile was not kept moist during construction, resulting in cracking of the pavement surface. Although this occurrence may have contributed to the onset of the distress by "opening" up the concrete surface, making it more permeable to water and deicers, it alone cannot be blamed for the observed distress at this time.

The deterioration has continued to progress over time, and in the most serious case has required removal and replacement of the highly deteriorated cross-over lanes after only nine years of service. The progression has not only appeared as cracking, but includes staining, spalling, and

[1] Depuy, G.W. (1994). "Chemical Resistance of Concrete." Concrete and Concrete Making Materials. STP 169C. American Society for Testing and Materials. Philadelphia, PA.

what can best be described as complete disintegration of the hydrated cement paste matrix. Microscopically, it is evident that significant infilling of the entrained air-void system has occurred and that in the deteriorated pavement sections, alkali-silica reactivity is causing fracturing of chert fine aggregate particles and subsequent microcracking of the paste. There are currently two hypotheses that are being considered to explain the observed deterioration. The first is that ASR is primarily responsible and the second is that the dissolution of the calcium sulfide found in the slag coarse aggregate is causing a type of internal sulfate attack from excess sulfates. Further, it is possible that both mechanisms are in conjunction with one another, or in combination with as yet unknown factors, such as the occurrence of the initial cracking. Each of these hypotheses is discussed below.

Alkali-Silica Reactivity

The first hypothesis is that ASR is the primary mechanism responsible for the observed deterioration. It is clear from the petrographic analysis that chert particles contained in the fine aggregate are reactive. Further, without exception, in pavements that are showing visible signs of materials-related distress (map cracking, staining, spalling, and deterioration), these fine aggregates are showing deleterious reactions in which the particles are fracturing and alkali-silica reaction product is being produced, filling cracks and nearby air voids. In contrast, in cores obtained from the three "fair" performing sections, few if any such deleterious reactions were observed.

Also supporting the ASR hypothesis is that the total alkali contents for the distressed sections of US-23N were in excess of that recommended for complete protection from ASR. Two of the cores (cores 38 and 22) were even in excess of the limit for mild ASR protection (maximum of 3.0 kg/m^3 Na_2O equivalent)[2]. Two of the distressed sections with lower total alkali content were older than the 1992 sections, and thus the reactions would have had longer to manifest themselves. In contrast, cores from the three fair performing sections all had total alkalis well below the recommended limits set for strong protection.

[2]Fournier, B., M. Bérubé, and C. A. Rogers (1999). *Proposed Guidelines for the Prevention of Alkali-Silica Reaction in New Concrete Structures*. Journal of the Transportation Research Board. No. 1668. Transportation Research Board. Washington, D.C.

But some problems exist with the ability of the ASR theory to completely explain all of the observations. The first is that the observed pavement deterioration is not completely consistent with that solely caused by ASR. Pavements affected by ASR will typically manifest map cracking with exudate, spalling, and evidence of expansion. The US-23N sections show some signs of map cracking (Figures 2 and 4), but little sign of exudates. Further, the observations of the complete deterioration of the hydrated cement paste, as shown in Figures 1 and 3, is inconsistent with deterioration caused by ASR. Another problem with the ASR theory is that the cracking became apparent within a few years of construction. This is an extremely short time frame for ASR, since it is commonly thought to take at least 5 years to become manifest, especially considering that the alkali contents were not extreme for most of the sections.

Another observation that does not support ASR as the exclusive distress mechanism is that the most severe deterioration was observed in the section from which core 15 (CS 25031-30798A) was obtained, yet this section did not have an excessively high total alkali content compared to some other sections, being at 2.1 kg/m^3 Na_2O equivalent. What is unique about this section was the use of a very high cement content at 502 kg/m^3 (9 sacks) and no fly ash. Based solely on the amount of total alkalis available, it seems likely that this section would have suffered less deterioration than that from which core 38 (CS 25031-30798A) was obtained (which had a total alkalinity of 4.3 kg/m^3 Na_2O equivalent), but the opposite is true.

It is also known from other work conducted at Michigan Tech that the reactivity problem with the chert particles in the fine aggregate seems to be most closely associated with concrete containing slag as a coarse aggregate. Further work needs to be done regarding this observation, as there seems to be some, as yet undefined, interaction between deleterious ASR and the presence of slag coarse aggregate.

Dissolution of Calcium Sulfide

Work conducted by Michigan Tech in the past has demonstrated through thermodynamic calculations and visual observations that calcium sulfide inclusions present in blast furnace slag

can be highly soluble in the highly alkali environment present in the concrete pore solution.[34] This dissolution can result in the secondary formation of ettringite and gypsum in available void space within the concrete. Ettringite filling the air-void system can potentially compromise its ability to protect the paste against freeze-thaw damage.[5] Of greater concern would be sulfate ions in solution, which could lead to direct sulfate attack of the hydrated cement paste. Evidence supporting this potential distress mechanism is the significant infilling of the air-void system with sulfate-bearing minerals that has been observed in all of the cores that were evaluated. Such infilling is a common feature of in-service concrete, particularly that which has deteriorated. But the infilling in the cores evaluated in this case study is excessive, even in concrete from pavements in "fair" condition. From the US-23N project, the two most severely deteriorated sections (cores 15 and 22 [both from CS 25031-30798A]) have existing spacing factors that would be classified as deficient with regards to freeze-thaw protection, even though the original spacing factors were adequate (see Figure 5). Interestingly, the other two sections having deficient air-void system both had deficient systems as constructed (cores 19b [CS 50011] and 1 [CS 25031-31018A]). Core 1 was obtained from a pavement considered to be in "fair" condition.

As was discussed, the percent of sulfate in excess of that calculated was significantly higher in the distressed pavement sections than in the pavements considered to be in fair condition. Core 15 (CS 25031-30798A), from the most deteriorated section, had the highest calculated and extracted sulfate content, with a percent excess sulfate of approximately 30 percent. The highest percentage of excess sulfate was measured in core 19b (CS 50011), which is from another highly distressed section. In contrast, the three cores (1, 1a, and 9)obtained from pavements in fair condition had significantly lower percentages of excess sulfate. There are too few data points and too many assumptions/factors to make definitive conclusions based on this analysis, but a trend does seem to be emerging that suggests that excess sulfates are contributing to the observed distress.

---

[3] Peterson, K.W., D. Hammerling, L.L. Sutter, T. J. Van Dam, and G.R. Dewey, "Oldhamite: Not Just in Meteorites," Proceedings of the 21st International Conference on Cement Microscopy, Las Vegas, NV, April 25-29, 1999.

[4] Hammerling, D., K.R. Peterson, L.L. Sutter, T. J. Van Dam, and G.R. Dewey, "Ettringite: Not Just in Concrete." Proceedings of the 22st International Conference on Cement Microscopy, Montreal, Canada. April 30 to May 4, 2000.

[5] Note that this result is hotly debated in the concrete literature and it is unclear whether air voids could fill sufficiently with secondary ettringite to prevent them from protecting against freeze-thaw damage.

As discussed, the sources of excess sulfate are most likely from other concrete constituents, such as the mixing water and aggregate. For the concrete under investigation, it is quite possibly the result of the dissolution of calcium sulfide and the formation of sulfate-bearing minerals. The solubility of calcium sulfide is directly related to the alkalinity of the pore solution, with higher pH values resulting in increased solubility[6]. Thus, higher alkalinity not only results in higher ASR potential, but would also increase the solubility of calcium sulfide. This is an important interaction and one that should be a focal point for future investigations into the deterioration of concrete containing slag coarse aggregate.

Other Factors

In addition to the two hypotheses described previously, other factors may have contributed to the deterioration either by acting in conjunction with the mechanisms cited or wholly on their own. A major unknown is the conditions present during construction. This relates to the construction process itself (e.g. materials handling, mixing, transporting, placing, and curing of concrete) as well as the ambient conditions that may have occurred during placement (e.g. temperature). It is well known that such conditions can have a significant impact on concrete durability either directly or indirectly. For example, high curing temperatures can lead to the formation of undesirable hydration products and/or desiccation of the surface resulting in cracking. Other factors resulting in an increase in permeability of the concrete will negatively impact its durability simply by allowing moisture and deicers more ready access. This is true for ASR and sulfate attack, both of which require water to facilitate ion transfer and for the transmission of expansive forces that fracture the concrete. Permeability can be negatively affected by many factors including material selection, mix proportions, mixing, placement, and curing. One question that needs to be resolved is whether the permeability of concrete using slag coarse aggregate differs significantly from that of concrete made with natural aggregate.

[6] Hammerling, D., K.R. Peterson, L.L. Sutter, T. J. Van Dam, and G.R. Dewey, "Ettringite: Not Just in Concrete." Proceedings of the 22st International Conference on Cement Microscopy, Montreal, Canada. April 30 to May 4, 2000.

Conclusions

Based on the results of this study, the following conclusions can be drawn:

- The results of the air-void system analysis found that most of the concrete originally had an air-void system that was adequate to protect the paste against freeze-thaw damage. Since construction, the air voids have been filling with secondary sulfate mineral deposits, which in some cases might be compromising the efficiency of the air-void system. This was most pronounced in the more seriously deteriorated pavement sections, but even one of the "fair" sections had a deficient air-void system.
- Petrographic evaluation of thin sections demonstrated conclusively that the chert particles in the fine aggregate are undergoing a deleterious alkali-silica reaction in all of the pavement sections classified as distressed. This reaction is characterized by fracturing of the aggregate particles, related fracturing of the surrounding paste, and the production of alkali-silica reaction product observed in cracks and voids. In contrast, examination of thin sections made from pavement sections classified as "fair" did not show similar deleterious deterioration. Although the chert particles were stained yellow by the indicator, little or no aggregate fracturing or reaction product formation was observed.
- The available total alkalis extracted from the various cores showed that in all but one case, the total alkalis measured from cores obtained from distressed pavements were in excess of the recommended limit for strong ASR protection. The two cores having the highest alkali content contained a Class C fly ash. In contrast, all of the cores obtained from fair performing pavements had total alkali contents lower than the limit for strong protection. Two of these sections were constructed with a Class F fly ash.
- The sulfate extraction tests performed indicated that the excess sulfate was significantly higher in cores obtained from distressed sections than that from pavements in fair condition. A source for the excess sulfate could not be unequivocally found, but it is likely that the dissolution of calcium sulfide in the slag coarse aggregate is contributing. The excess sulfate could contribute to the formation of sulfate-bearing minerals (e.g. ettringite) in the available air-void space, potentially compromising its ability to protect the paste against freeze-thaw damage. Further, excess sulfate may be leading to internal sulfate attack of the hydrated cement paste. This dissolution process is directly dependent upon the alkalinity of the pore

solution. Thus there is an interaction between the potential for ASR and dissolution of calcium sulfide.

- In reviewing all available data, there is no definitive single cause that can be forwarded at this time regarding the deterioration observed on US-23N. Two hypotheses have emerged that can at least partially explain the deterioration, and it is possible that the two may be acting together to contribute to the observed deterioration. The first hypothesis focuses on the alkali-silica reactivity of the chert particles in the fine aggregate, which is aggravated by the total alkalinity in the concrete and Class C fly ash. The presence of the Class F fly ash appears to offer a mitigating effect. The second hypothesis focuses on the dissolution of the calcium sulfide and the formation of sulfate-bearing minerals, which results in a type of internal sulfate attack. Construction factors may also play a role, particularly with relation to rate of distress formation and severity.

Appendix A

Coring and Mixture Design Information as Provided by MDOT for US-23 N and US-23S Projects

Coring on US-23 Just South of Flint

May 30, 2001

Mix #1 and #2 were from a concrete job done one year after (1993) the job of interest. This section of pavement is in very good condition.

Mix #1: 35P with some fly ash, in the right lane near the on-ramp from the Rest Area (Cores 1-7).

Mix #2: 35HE in the shoulder adjacent to area with Mix #1 (Cores 8-14).

Mixes #3 through #6 are all on the pavement that was built in 1992. This pavement is in varying states of distress. The distress is primarily a crumbling at the joints.

Mix #3: 9 sack fast-set. Primarily used in short sections for crossovers. These sections are in very poor condition (Cores 15-21).

Mix #4: 35P with some fly ash. The area where the cores were taken had some deterioration as the joints, however the cores for MRD analysis were taken at a joint in relatively good condition (Cores 22-28).

Mix #5: 35P without fly ash. This concrete is in pretty good condition with a minimal amount of deterioration (Cores 29-35).

Mix #6: 35P with more fly ash than mix #4. The concrete in this area is in good condition (Cores 36-42).

There are a number of longitudinal cracks within a foot of the centerline joint throughout the entire job. They are prevalent in any one mix design.

Mix design information for all mixes except #3 are attached. Also attached are mill certs for the fly ash used on the 1992 job.